72 Polymer ferroelectrics

No. 72-1 $(CH_2CF_2)_n$, Polyvinylidene fluoride (PVDF, PVF_2)

1a Large piezoelectric effect was observed in melt-quenched and uniaxially-drawn films of PVDF by Kawai in 1969. Pyroelectricity was found by Bergman et al. in 1971. Ferroelectricity in the thickness direction was confirmed by square hysteresis loops by Kepler et al. in 1978, and by switching current by Furukawa et al. in 1981. 69Kaw 71Ber 78Kep2 81Fur

b Crystalline PVDF has at least four different modifications: I(β), II(α), III(γ) and IV(α_p). Cooling from the melt yields form II. Uniaxial drawing converts form II into I which is ferroelectric. Annealing at high temperatures converts form II into III. Poling at ≈1.2 · 10^8 Vm^{-1} converts form II into IV. 78Dav 81Lov 95Tas

phase	I(β)	II(α)	III(γ)	IV(α_p)
state	F			
crystal system	orthorhombic	monoclinic	orthorhombic	monoclinic
space group	$Cm2m - C_{2v}^{14}$	$P2/c - C_{2h}^{4}$	$Cc - C_{s}^{4}$	$P2_1cn - C_{2v}^{9}$
conformation *	all-trans	$TGT\overline{G}$	$T_3GT_3\overline{G}$	$TGT\overline{G}$
packing	parallel	anti-parallel	parallel	parallel

* T: trans; G: gauche; $\overline{G}$: gauche minus.

2a Melt-solidified or solvent-cast film was subjected to uniaxial-drawing 4...5 times the length at 60...80 °C. The degree of crystallinity was usually 40...60 %. 69Kaw 72Has 75Kob

3a Unit cell parameters of form I: a = 8.58 Å, b = 4.91 Å, c = 2.56 Å. 72Has

b Structure of form I PVDF: Fig. 72-1-001. 72Has
Coordinate system in uniaxially-drawn and poled films: X, draw direction; Z, thickness direction; Y, orthogonal to X and Z. 72Has
The mean directions of a, b and c axes of the crystalline regions in the form I (orthorhombic) are approximately parallel to Y, Z and X axes, respectively. 72Has
The ferroelectric axis is b.

5a Dielectric properties: see 80Miy
Dielectric constant vs. temperature: Fig. 72-1-002.

b Nonlinear dielectric properties: see 87Fur
κ vs. E and D vs. E hysteresis loops: Fig. 72-1-003.

c $P_r = 6 \cdot 10^{-2}$ C/m^2, $E_c = 5 \cdot 10^7$ $V\ m^{-1}$. 80Fur
D-E hysteresis loops: Fig. 72-1-004.
Switching characteristics: Fig. 72-1-005.
Larger P_r reaching 10^{-1} $C\ m^{-2}$ is reported for deuterated or high pressure crystallized PVDF. 87Tak3, 96Hat

d $p_3 = 3 \cdot 10^{-2}$ $C\ m^{-2}\ K^{-1}$. 89Fur
p_3 vs. P_r: see Fig. 72-2-022.

6a Heat capacity: Fig. 72-1-006.

7a	Piezoelectric constants vs. P_r at 10 Hz: Fig. 72-1-007.	
	Piezoelectric matrix: Table 72-1-001; see also	78Kep1
b	Electrostriction $Q_{33} = -2.4$ m^4/C^2.	90Fur
8a	Elastic matrix: Table 72-1-002.	
9a	Refractive indices: $n_1 = 1.448$, $n_2 = 1.414$, $n_3 = 1.412$.	90Ogu
b	Electrooptic effect: see	80Bro, 80Ohm, 84Goo
c	Piezooptic effect: see	80Bro
e	Nonlinear optical coefficient: $d_{31} \approx (1/2)d_{11}$ (SiO_2), $d_{33} \approx d_{11}$ (SiO_2).	71Ber
10a	LO-TO splitting in PVDF: see	85Tas
16	Poling-induced structural changes: see	92Kep, 87Tak2, 86Bur
	Electric-field-induced dipole orientation: see	77Tam, 78Nae, 83Lat
	X-ray anomalous scattering: see	87Tak2
	Twin structure: see	87Tak1

Table 72-1-001. PVDF. Piezoelectric matrix components of uniaxially-drawn and poled films [88Nix]. $d_{i\lambda}$: [· 10^{-12} CN^{-1}], $e_{i\lambda}$: [· 10^{-3} C m^{-2}].

(a) Static measurements.

d_{31}	d_{32}	d_{33}	d_{15}	d_{24}
21	1.5	–32.5	–27	–23

(b) At resonant frequency *f*.

	d_{31}	d_{32}	e_{33}	e_{15}	e_{24}
	19	3	–125	–15	–48
f [MHz]	0.1	0.1	30	0.3	0.3

Table 72-1-002. PVDF. Elastic matrix components of uniaxially-drawn and poled films [96Omo]. $s_{\lambda\mu}$: [· 10^{-9} N^{-1} m^2], $c_{\lambda\mu}$: [· 10^9 N m^{-2}].

(a) Static measurements.

s_{11}	s_{22}	s_{33}	s_{21}	s_{31}	s_{32}
0.32	0.40	0.68	–0.06	–0.21	–0.25

(b) At resonant frequency *f*.

	$1/s_{11}$	$1/s_{22}$	c_{33}	c_{44}	c_{55}
	4.5	5.14	8.62	1.61	1.12
f [MHz]	0.1	0.1	30	0.3	0.3

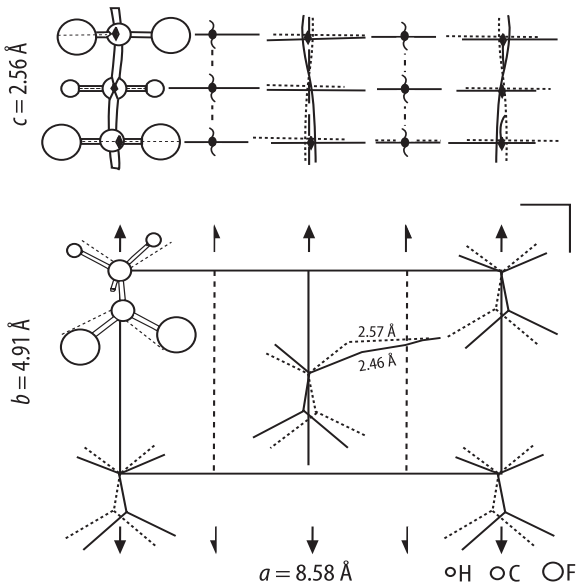

Fig. 72-1-001. PVDF. There is statistical disorder in crystal structure of form I [72Has]. Solid and dotted lines show two possible molecular positions.

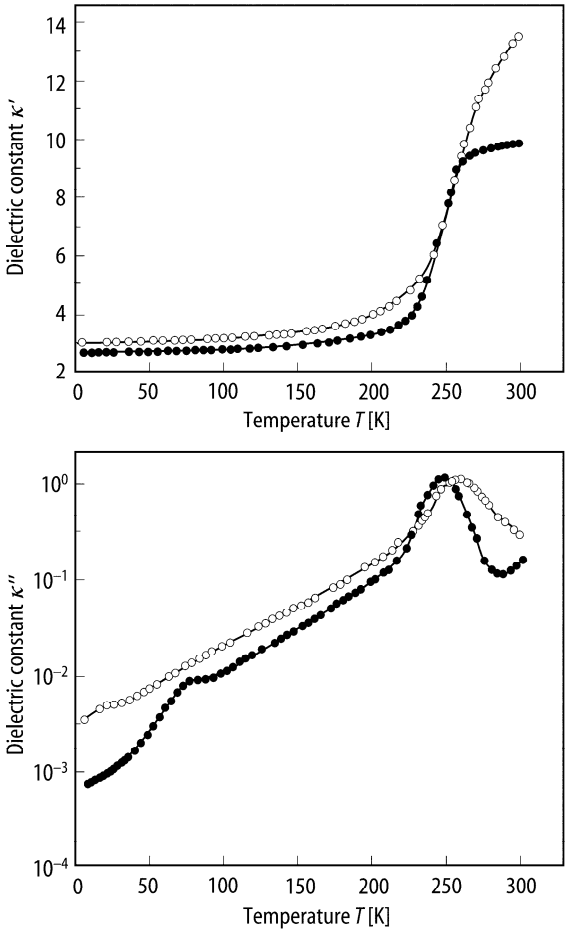

Fig. 72-1-002. PVDF. κ', κ'' vs. T for form I (full circle) and form II (open circle) at 1 kHz [81Ari].

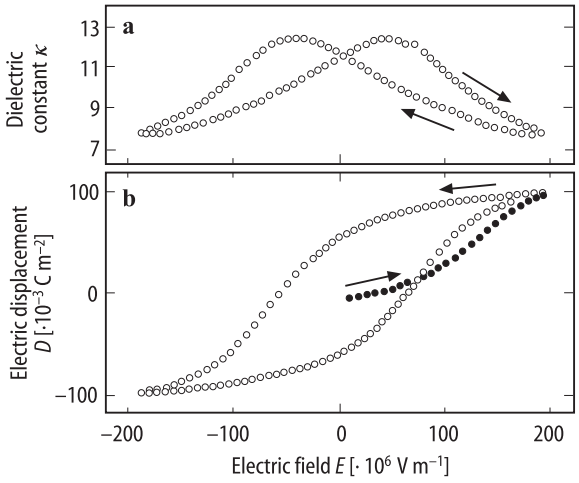

Fig. 72-1-003. PVDF. (**a**) κ vs. E and (**b**) D vs. E hysteresis loop [80Tak]. Full circle: for the applied field initially, open circle: for the 10th cycle of the applied field.

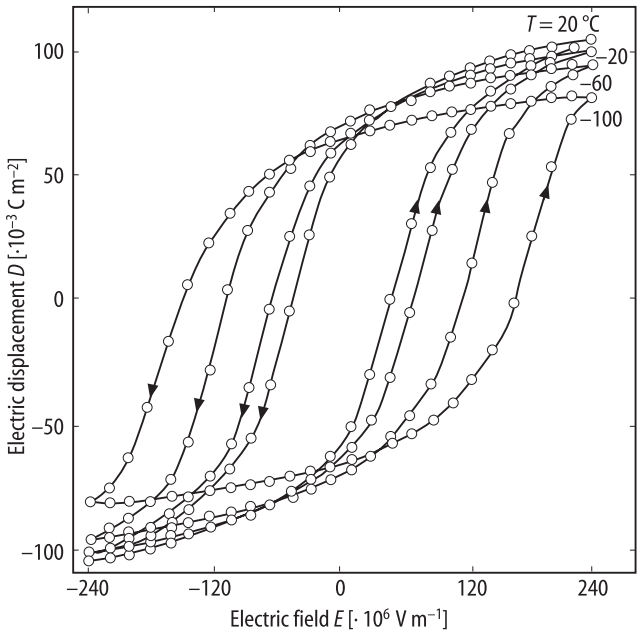

Fig. 72-1-004. PVDF. D vs. E hysteresis loops of uniaxially-drawn film [80Fur]. Parameter: T.

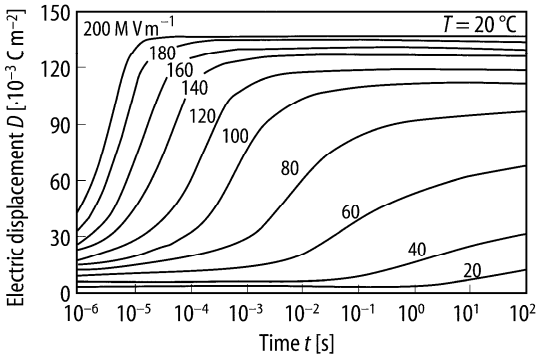

Fig. 72-1-005. PVDF. Ferroelectric switching characteristics measured under step-fields of 20 to 200 MVm^{-1} at 20 °C [81Fur].

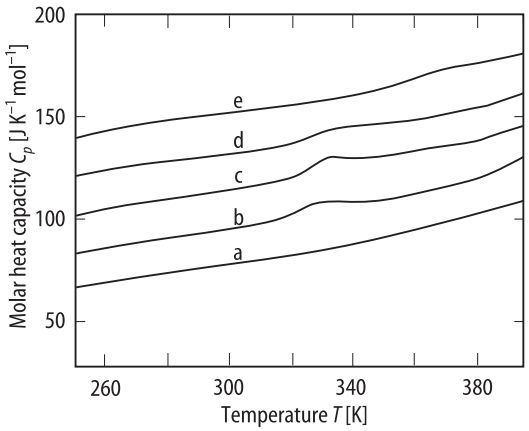

Fig. 72-1-006. PVDF. DSC chart with different thermal histories [87Lou]. Consecutive curves are shifted by 18 JK^{-1}mol^{-1}. Curve a: cooled from the melt at 10 K min^{-1}, b: quickly cooled from the melt, c: quenched from the melt into liq. N_2, d: isothermally crystallized at 440 K, e: annealed for two days by cooling slowly from 335 to 315 K.

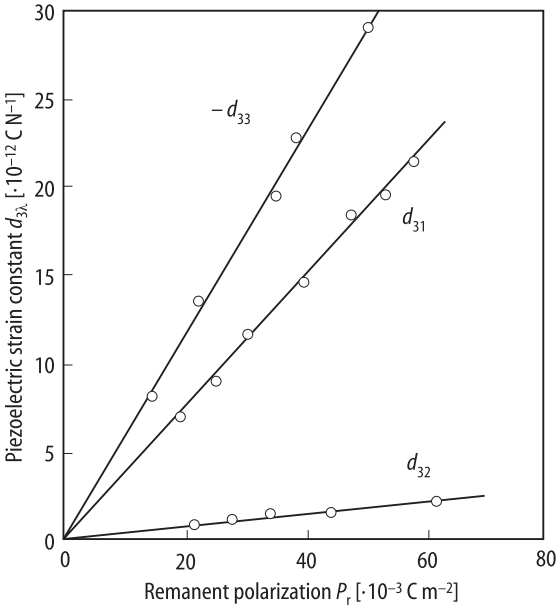

Fig. 72-1-007. PVDF. d_{31}, d_{32}, d_{33} vs. P_r at 10 Hz [89Fur].

References

69Kaw Kawai, H.: Jpn. J. Appl. Phys. **8** (1969) 975.
71Ber Bergman, J.G., MacFee, J.H., Crane, G.R.: Appl. Phys. Lett. **18** (1971) 203.
72Has Hasegawa, R., Takahashi, Y., Chatani, Y., Tadokoro, H.: Polym. J. **3** (1972) 600.
75Kob Kobayashi, M., Tashiro, K., Tadokoro, H.: Macromolecules **8** (1975) 158.
77Tam Tamura, M., Hagiwara, S., Matsumoto, S., Ono, N.: J. Appl. Phys. **48** (1977) 513.
78Dav Davis, G.T., McKinney, J.E., Broadhurst, M.G., Roth, S.C.: J. Appl. Phys. **49** (1978) 4998.
78Kep1 Kepler, R.G., Anderson, R.A.: J. Appl. Phys. **49** (1978) 4490.
78Kep2 Kepler, R.G.: Org. Coating Plast. Chem. **38** (1978) 706.
78Nae Naegele, D., Yoon, D.Y.: Appl. Phys. Lett. **33** (1978) 132.
80Bro Broussoux, D., Micheron, F.: J. Appl. Phys. **51** (1980) 2020.
80Fur Furukawa, T., Date, M., Fukada, E.: J. Appl. Phys. **51** (1980) 1135.
80Miy Miyamoto, Y., Miyaji, H., Asai, K.: J. Polym. Sci.: Polym. Phys. Ed. **18** (1980) 597.
80Ohm Ohmori, Y., Yoshino, K., Inuishi, Y.: Jpn. J. Appl. Phys. **19** (1980) 263.
80Tak Takahashi, T., Date, M., Fukada, E.: Appl. Phys. Lett. **37** (1980) 791.
81Ari Arisawa, H., Yano, O., Wada, Y.: Ferroelectrics **32** (1981) 39.
81Fur Furukawa, T., Johnson, G.E.: Appl. Phys. Lett. **38** (1981) 1027.
81Lov Lovinger, A.: Developments in Crystalline Polymers - 1, Bassett, D.C. (ed.), London: Applied Science Publications Ltd., 1981, p. 195.
83Lat Latour, M., Abodorra, H., Galigne, J.L.: J. Polym. Sci. **22** (1983) 345.
84Goo Gookin, D., Morris, R.: Appl. Phys. Lett. **45** (1984) 603.
85Tas Tashiro, K., Itoh, Y., Kobayashi, M., Tadokoro, H.: Macromolecules **18** (1985) 2600.
86Bur Bur, A.J., Barnes, J.D., Wahlstrand, K.J.: J. Appl. Phys. **59** (1986) 2345.
87Fur Furukawa, T., Nakajima, K., Koizumi, T., Date, M.: Jpn. J. Appl. Phys. **26** (1987) 1039.
87Lou Loufakis, K., Wunderlich, B.: Macromolecules **20** (1987) 2474.
87Tak1 Takahashi, N.: Appl. Phys. Lett. **51** (1987) 970.
87Tak2 Takahashi, Y., Nakagawa, Y., Miyaji, H., Asai, K.: J. Polym. Sci. Part C **25** (1987) 153.
87Tak3 Takase, Y., Tanaka, H., Wang, T.T., Cais, R.E., Kometani, J.M.: Macromolecules **20** (1987) 2318.
88Nix Nix, E.L., Nanayakkara, J., Davies, G.R., Ward, I.M.: J. Polym. Sci. Part B **26** (1988) 127.
89Fur Furukawa, T.: IEEE Trans. Electr. Insul. **24** (1989) 375.
90Fur Furukawa, T., Seo, N.: Jpn. J. Appl. Phys. **29** (1990) 675.
90Ogu Ogura, H., Kase, K.: Ferroelectrics **110** (1990) 145.
92Kep Kepler, R.G., Anderson, R.A.: Adv. Phys. **41** (1992) 1.
95Tas Tashiro, K.: Ferroelectric Polymers, Nalwa, H.S. (ed.), New York: Marcel Dekker, 1995, p. 66.
96Hat Hattori, T., Kanaoka, M., Ohigashi, H.: J. Appl. Phys. **79** (1996) 2016.
96Omo Omote, K., Ohigashi, H.: Jpn. J. Appl. Phys. **35** (1996) 1818.

No. 72-2 $((CH_2CF_2)_x(CHF{\cdot}CF_2)_{1-x})_n$, Vinylidene fluoride-trifluoroethylene copolymer (VDF_x–$TrFE_{1-x}$, VDF–TrFE)

1a Ferroelectric hysteresis loops were observed in films of random copolymers $((CH_2CF_2)_x(CF_2CHF)_{1-x})_n$ for x > 0.5 by Furukawa et al. and Yagi et al. in 1980. 80Fur, 80Yag

b

phase	II	I
state	F	P
crystal system	orthorhombic	hexagonal
conformation *	all-trans	random mixture of TT, TG, T$\overline{G}$

89Tas

* T: trans; G: gauche; $\overline{G}$: gauche minus.

Ferroelectric transition temperature appears below T_{melt} for 0.5 < x < 0.8. 80Kit
Phase diagram: Fig. 72-2-001.

2a Films 10...100 μm in thickness are produced by melt-solidification or solvent-casting. Uniaxial-drawing is not necessary for obtaining ferroelectric film. Spin-coat technique is useful for producing very thin films (50 nm...10 μm). 80Kit, 83Kim

b Crystal forms of VDF_x–$TrFE_{1-x}$ with 0.5 < x < 0.8 89Tas

3a (110), (200) spacing vs. x: Fig. 72-2-002.
c = 2.56 Å in F and c = 2.30 Å in P state. 82Lov, 83Lov1, 83Lov2

Lattice spacing depends upon not only composition but also crystallization temperature, annealing condition, uniaxial-drawing and poling. 84Tas, 89Tas

4 Thermal expansion of isotropic bulk: Fig. 72-2-003.
Thermal contraction of oriented film: Fig. 72-2-004.
$\Delta d_{110}/d_{110}$ (or $\Delta d_{200}/d_{200}$) vs. T: Fig. 72-2-005.
Temperature variation of (001) reflection: Fig. 72-2-006.
a vs. p: Fig. 72-2-007.

5a Dielectric properties, for a review see 84Fur1, 84Koi

Dielectric constants: Fig. 72-2-008.
Dielectric spectra: Fig. 72-2-009.
Dielectric loss in the far IR region: Fig. 72-2-010.
Dielectric anisotropy: Fig. 72-2-011.
Relaxation time: Fig. 72-2-012.
Effect of p on $1/\kappa'$ vs. T: Fig. 72-2-013.
Θ_{II-I} and T_{melt} vs. p: Fig. 72-2-014.

b Bias-field dependence of dielectric anomaly: Fig. 72-2-015.
C = 3800 K, $\xi = -1.5 \cdot 10^{12}$ V m^5 C^{-3}, $\zeta = 1.9 \cdot 10^{14}$ V m^9 C^{-5}. 84Fur2
Second nonlinear permittivity: Fig. 72-2-016.

c D vs. E hysteresis loop: Fig. 72-2-017.
Spontaneous polarization: Fig. 72-2-018.
Switching characteristics: Fig. 72-2-019.
Characteristic hysteresis loops in $VDF_{0.47}$–$TrFE_{0.53}$: Fig. 72-2-020.
P_r vs. x: Fig. 72-2-021.

d p_3 vs. P_r: Fig. 72-2-022.

6a	Adiabatic and ac specific heat: Fig. 72-2-023; see also Transition heat and entropy: Table 72-2-001.	92Miz
7a	d_{31}/s_{11}, d_{32}/s_{22} vs. P_r: Fig. 72-2-024. k_t vs. P_r: Fig. 72-2-025. Coupling factor vs. T: Fig. 72-2-026. Piezoelectric constants vs. T: see	92Gue
b	Electrostriction: $Q_{33} = -2.2$ m^4/C^2. Thickness change vs. voltage: Fig. 72-2-027.	90Fur
8a	Elastic constants: Table 72-2-002. Bulk modulus: Fig. 72-2-028. Temperature dependence of c_{ii} and $1/s_{ii}$: Fig. 72-2-029.	
9a	Refractive indices: Fig. 72-2-030.	
b	Electrooptical coefficient: $\chi_c = 0.4 \cdot 10^{-12}$ m V^{-1} uniaxially-drawn film (x = 0.75), $\chi_c = 1.4 \cdot 10^{-12}$ m V^{-1} single-crystal-like film (x = 0.75).	97Taj
e	Second harmonic coefficient: $d_{31} = 0.22 \cdot 10^{-12}$ mV^{-1}, $d_{33} = 4.3 \cdot 10^{-12}$ mV^{-1}.	89Ber
13a	NMR, for a review, see	85Leg, 86Ish1, 86Ish2, 87Hir, 89Per
	T_1, T_2 $T_{1\rho}$ vs. temperature for $VDF_{0.55}$–$TrFE_{0.45}$: Fig. 72-2-031. Second moment of magnetic resonance and mobile fraction vs. T for $VDF_{0.73}$–$TrFE_{0.27}$: Fig. 72-2-032. T_1, $T_{1\rho}$ vs. ν for $VDF_{0.7}$–$TrFE_{0.3}$: Fig. 72-2-033.	
14	X-ray meridional reflection: see Fig. 72-2-006 in subsection 4.	
16	Annealing effect on long period: Fig. 72-2-034. Annealing effect on Θ_{II-I}: Fig. 72-2-035. Annealing effect, see also	94Kim, 87Fer
	Crystallization condition: see	88Sta
	Anomalous scattering: Fig. 72-2-036. Domain rotation: see	92Day
	Microstructure: see	95Sas
	Radiation effect: see	91Dau

Table 72-2-001. VDF_x–$TrFE_{1-x}$. Transition heat ΔH and transition entropy ΔS at x = 0.70 and 0.80 [94Bel].

x	ΔH [10^3 J kg^{-1}]	ΔS [10^3 J kg^{-1} K^{-1}]
0.70	65	33
0.80	0.16	0.09

Table 72-2-002. VDF_x–$TrFE_{1-x}$. Elastic constants. A: unoriented film (x = 0.7) measured by time of flight of acoustic wave [95Isn]. B: oriented film (x = 0.7) measured by Brillouin scattering [93Kru]. C: oriented film (x = 0.75) measured by piezoelectric resonance [95Omo]. D: single-crystal-like film (x = 0.7) measured by piezoelectric resonance [97Omo].

	c_{11}	c_{22}	c_{33}	c_{12}	c_{13}	c_{23}	c_{44}	c_{55}	c_{66}
	[10^9 Nm^{-2}]								
A	9.73	9.73	9.98	6.03	6.41	6.41	2.07	2.07	1.85
B	15.71	9.53		6.10					2.02
C	$1/s_{11}$: 5.91	$1/s_{22}$: 4.81	11.1				2.59	2.49	
D	$1/s_{11}$: 27.7	$1/s_{22}$: 6.3	11				2.5	2.2	3.1

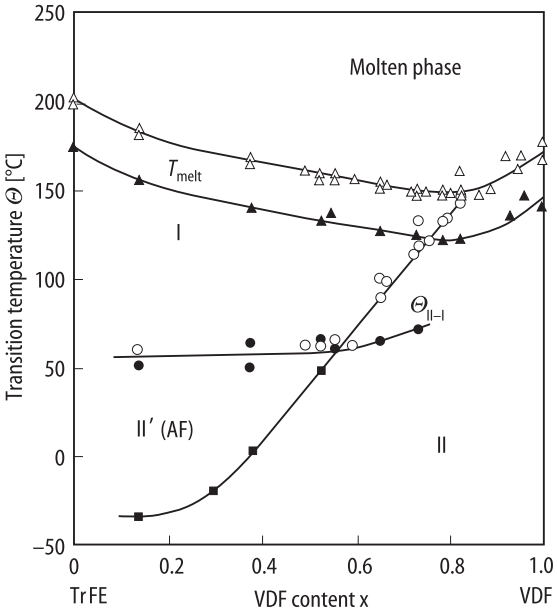

Fig. 72-2-001. VDF_x–$TrFE_{1-x}$. Phase diagram, Θ vs. x [89Fur2, 89Tas, 90Kog]. Open triangle: T_{melt} (heating); full triangle: T_{melt} (cooling); open circle: Θ_{II-I} or $\Theta_{II'-I}$ (heating); full circle: Θ_{II-I} or $\Theta_{II'-I}$ (cooling); full square: $\Theta_{II-II'}$ (heating). Clear indication of Θ_{II-I} is seen for $0.5 < x < 0.8$. For $x > 0.8$, Θ_{II-I} is overtaken by T_{melt}. Antiferroelectric-like hysteresis loop is observed in II′ for $0.3 < x < 0.5$ [86Koi].

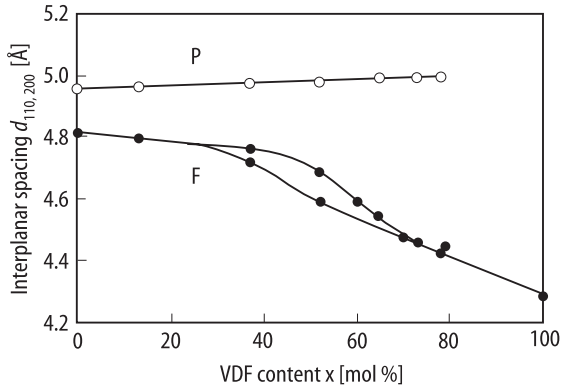

Fig. 72-2-002. VDF_x–$TrFE_{1-x}$. d_{110} (or d_{200}) vs. x in F (T = 20 °C) and P (T = 140 °C) phases [89Fur2, 94Bel]. In the intermediate composition (x = 0.3...0.7), a well ordered F phase and a less ordered F phase coexist.

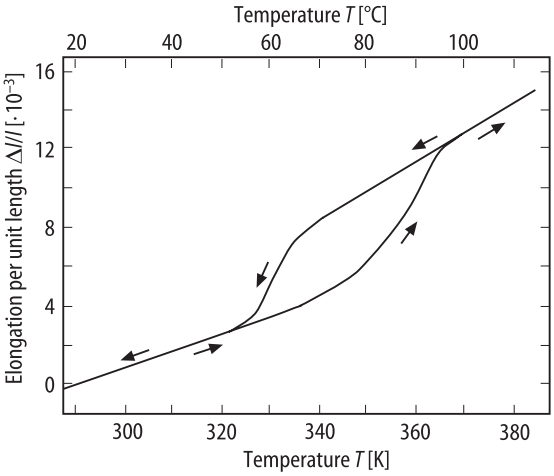

Fig. 72-2-003. $VDF_{0.65}$–$TrFE_{0.35}$. $\Delta l/l$ vs. T [84Koi].

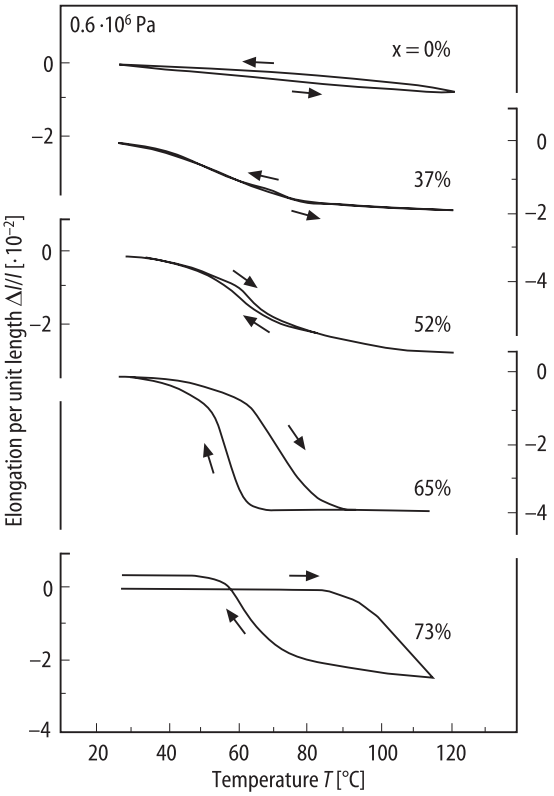

Fig. 72-2-004. VDF_x–$TrFE_{1-x}$. $\Delta l/l$ vs. T along the chain (draw) direction [88Tas]. Parameter: x.

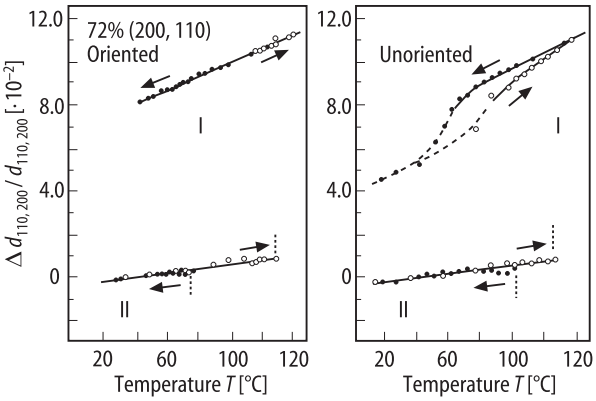

Fig. 72-2-005. $VDF_{0.72}$–$TrFE_{0.28}$. $\Delta d_{110,200}/d_{110,200}$ vs. T [84Tas]. Full circle: cooling, open circle: heating. I: paraelectric, II: ferroelectric.

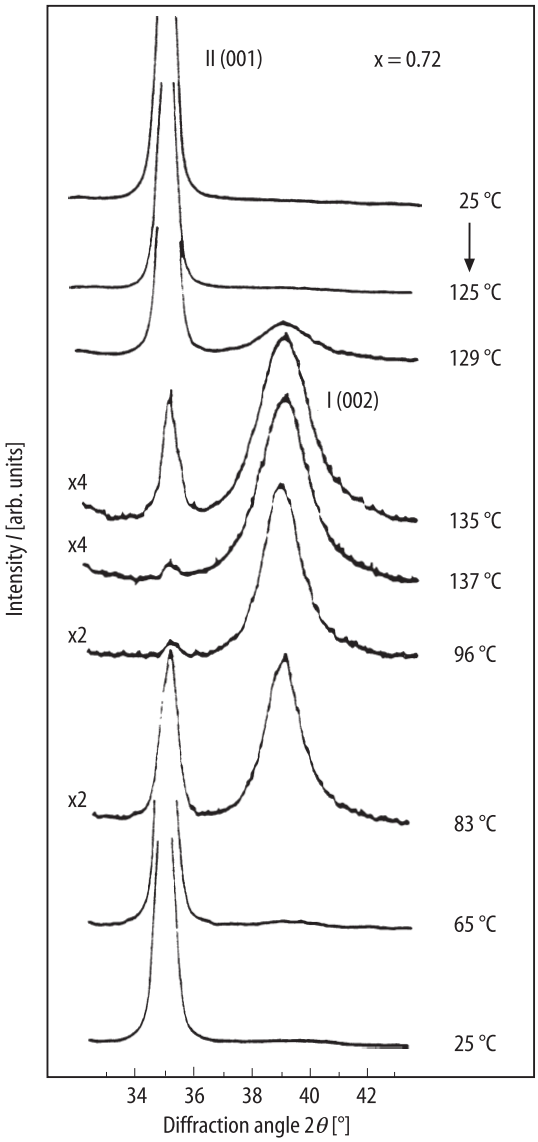

Fig. 72-2-006. $VDF_{0.72}$–$TrFE_{0.28}$. *I* vs. 2θ [89Tas]. Parameter: *T*. *I*: X-ray intensity of meridional (00l) reflection. 2θ: diffraction angle.

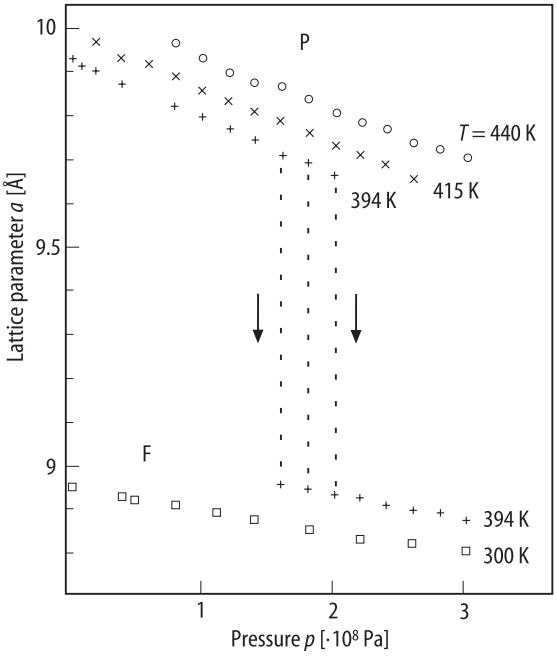

Fig. 72-2-007. VDF_x–$TrFE_{1-x}$. *a* vs. *p* at elevated temperatures [90Leg]. Pressure induced ferroelectric transition is observed at 394 K.

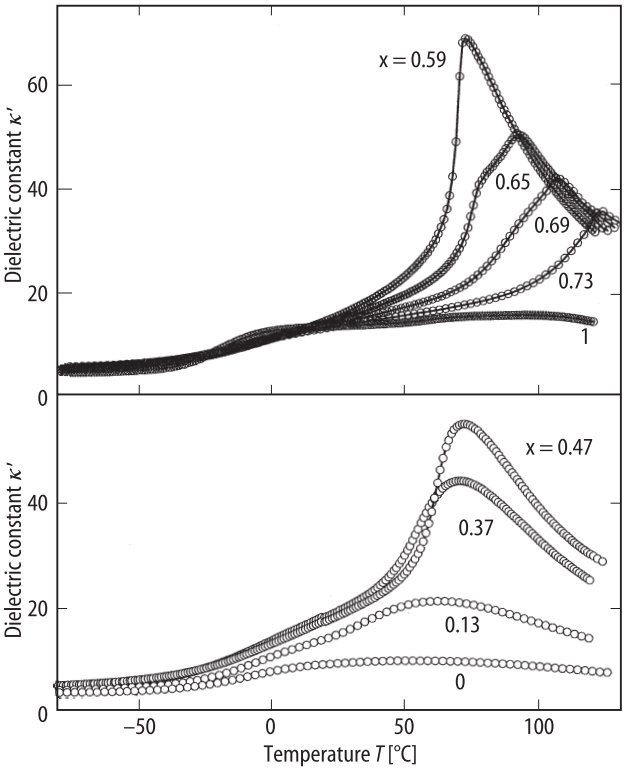

Fig. 72-2-008. VDF_x–$TrFE_{1-x}$. κ' vs. *T* [01Fur]. Parameter: x. *f* = 1 kHz. Thickness of specimen film = 50 μm.

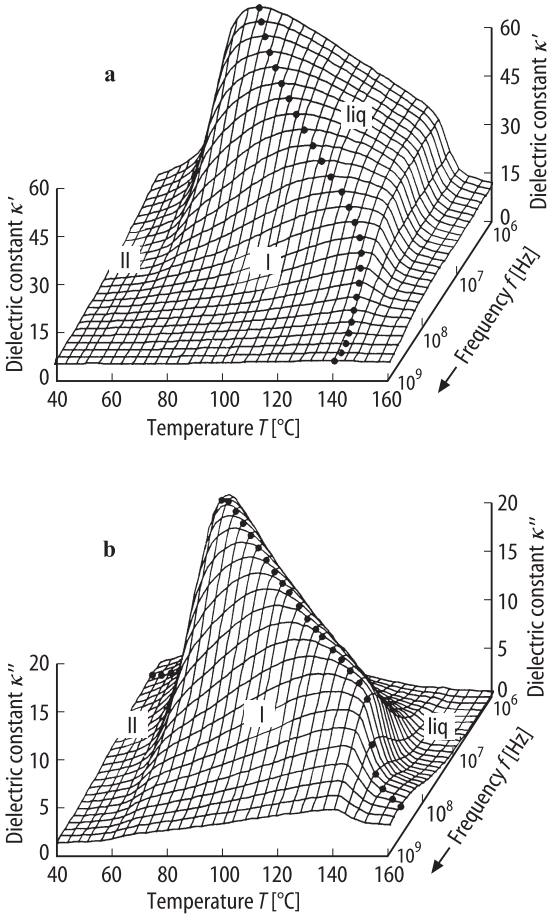

Fig. 72-2-009. $VDF_{0.65}$–$TrFE_{0.35}$. 3D plot of (**a**) κ' vs. T and f, (**b**) κ'' vs. T and f [89Fur2].

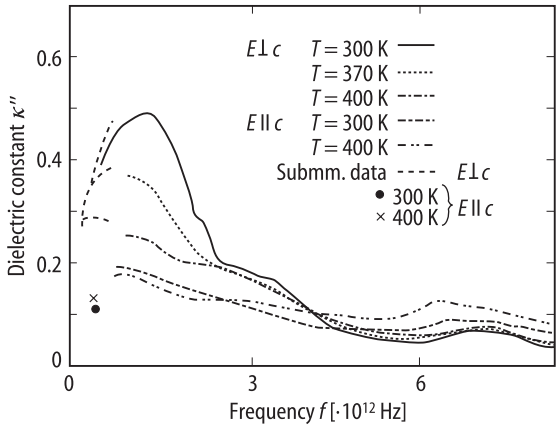

Fig. 72-2-010. $VDF_{0.7}$–$TrFE_{0.3}$. κ'' vs. f in the far-infrared and submillimeter regions [88Pet]. Parameter: T and direction.

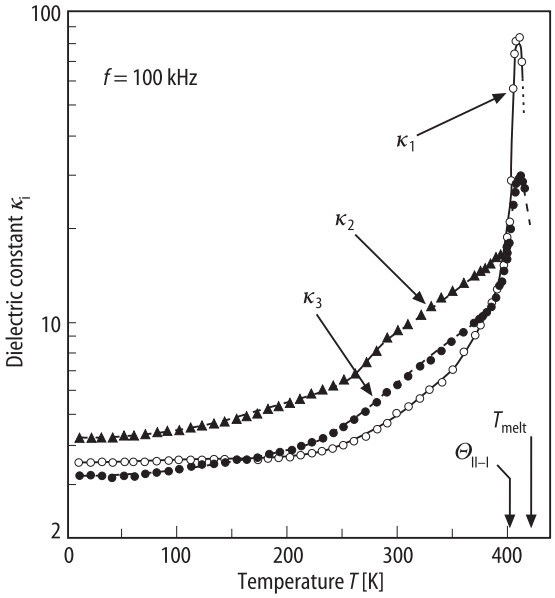

Fig. 72-2-011. $VDF_{0.75}$–$TrFE_{0.25}$. κ_1, κ_2, κ_3 vs. T of single-crystal-like film [97Omo].

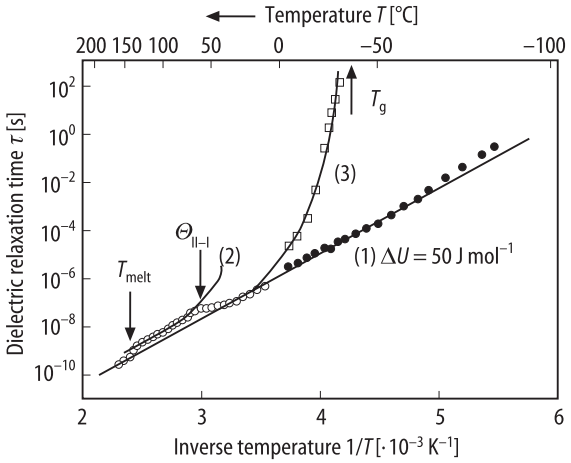

Fig. 72-2-012. $VDF_{0.65}$–$TrFE_{0.35}$. Transition map (τ vs. $1/T$) [92Fur]. τ: dielectric relaxation time. (1) Local crystalline motion, (2) cooperative crystalline motion, (3) segmental motion.

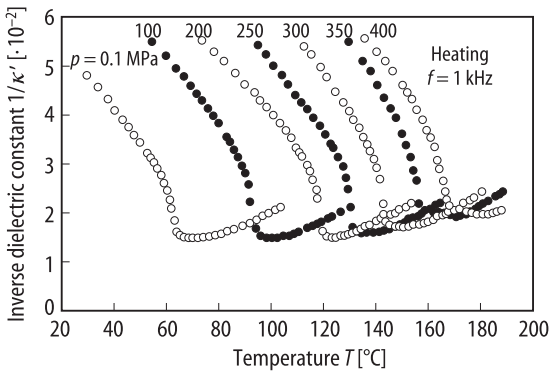

Fig. 72-2-013. $VDF_{0.54}$–$TrFE_{0.46}$. $1/\kappa'$ vs. T [89Mat]. Parameter: p.

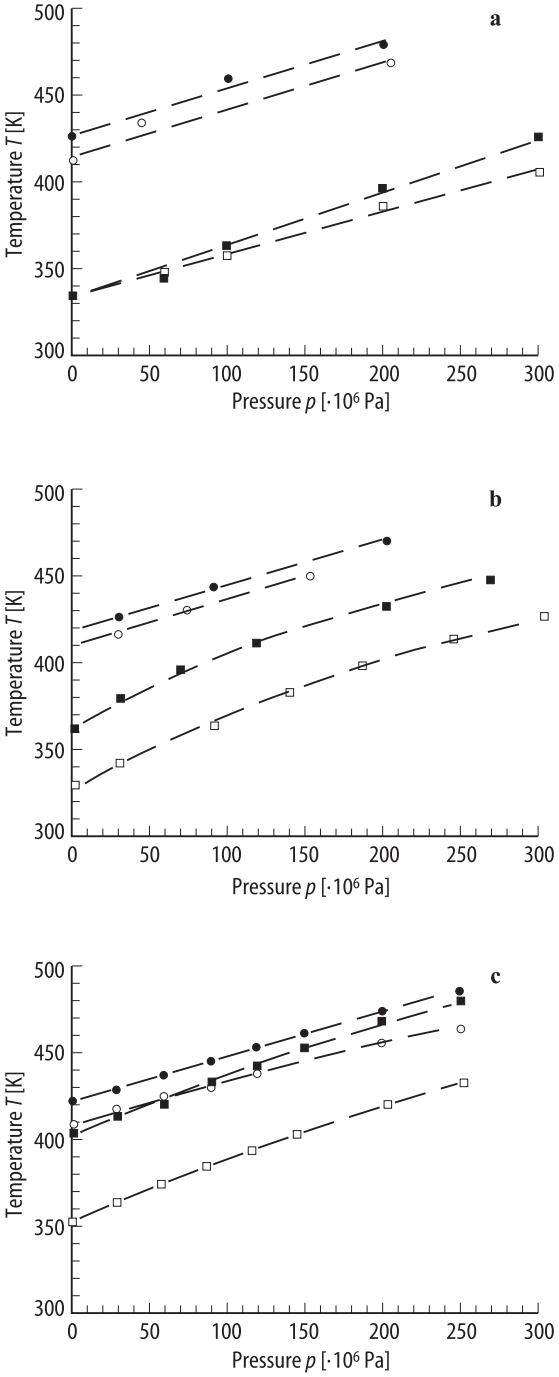

Fig. 72-2-014. VDF_x–$TrFE_{1-x}$. Θ_{II-I} and T_{melt} vs. p [94Bel]. Full square: Θ_{II-I} upon heating, open square: Θ_{II-I} upon cooling, full circle: T_{melt}, open circle: crystallization temperature. (**a**) x = 0.6, (**b**) x = 0.7, (**c**) x = 0.8.

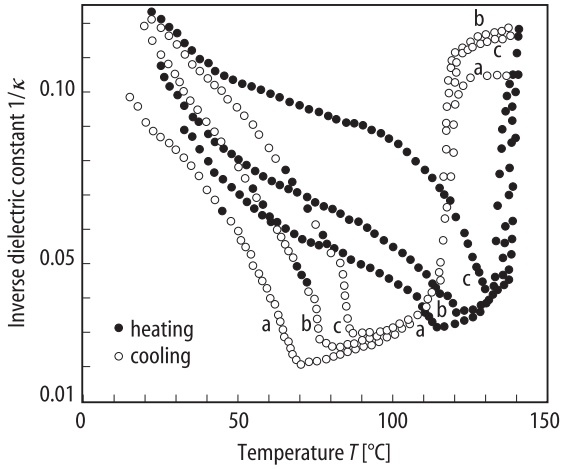

Fig. 72-2-015. $VDF_{0.74}$–$TrFE_{0.26}$. $1/\kappa$ vs. T [83Kim]. Parameter: bias field. Curve a: $E = 0$, b: $E = 27$ MV/m, c: $E = 44$ MV/m.

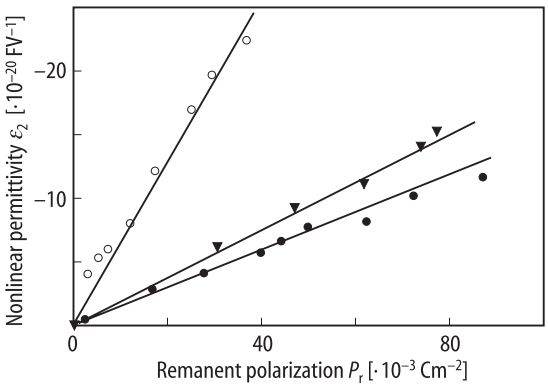

Fig. 72-2-016. VDF_x–$TrFE_{1-x}$. Second nonlinear permittivity ε_2 vs. P_r [91Ike]. $D = \varepsilon_1 E + \varepsilon_2 E^2$. Open circle: x = 0.52, full downside triangle: x = 0.65, full circle: x = 0.73.

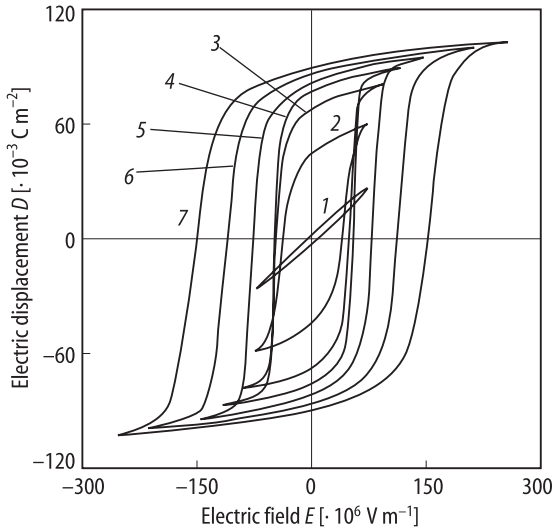

Fig. 72-2-017. $VDF_{0.65}$–$TrFE_{0.35}$. D vs. E hysteresis loops [89Fur2]. Parameter: T. (*1*) $T = 100$ °C, (*2*) 80 °C, (*3*) 50 °C, (*4*) 20 °C, (*5*) –10 °C, (*6*) –40 °C, (*7*) –70 °C.

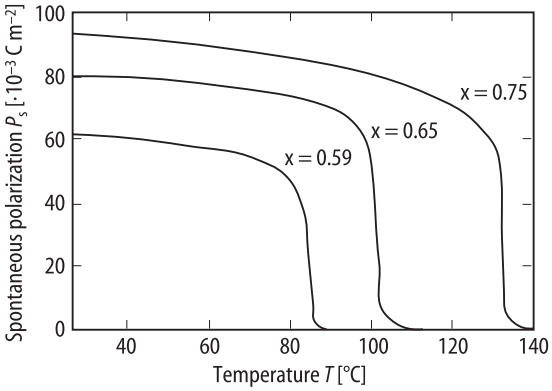

Fig. 72-2-018. VDF_x–$TrFE_{1-x}$. P_s vs. T [01Fur]. Parameter: x. f = 1 kHz. Thickness of specimen film = 50 μm.

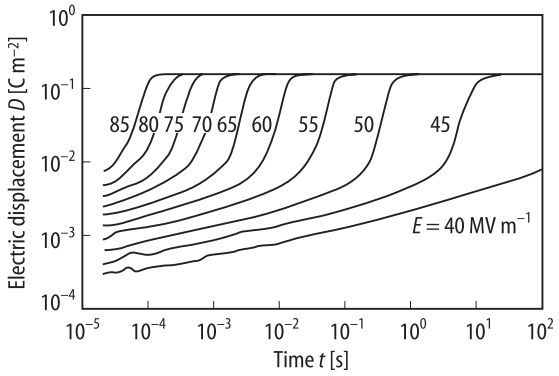

Fig. 72-2-019. $VDF_{0.65}$–$TrFE_{0.35}$. Switching characteristics [95Fur]. Parameter: E.

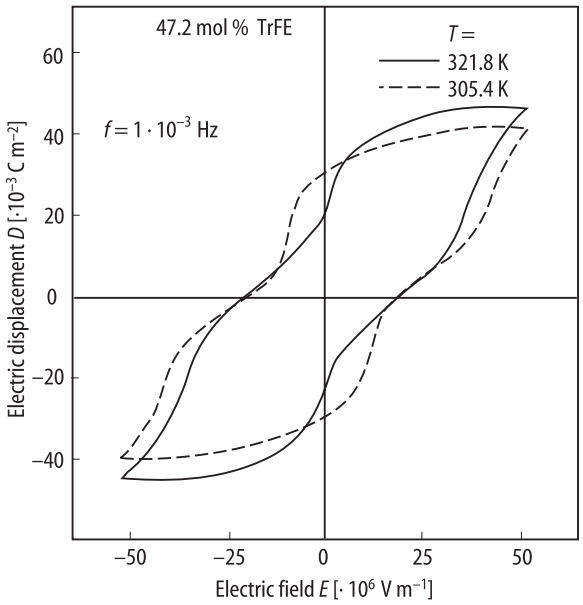

Fig. 72-2-020. $VDF_{0.47}$–$TrFE_{0.53}$. Characteristic hysteresis loops suggesting antiferroelectricity [86Koi].

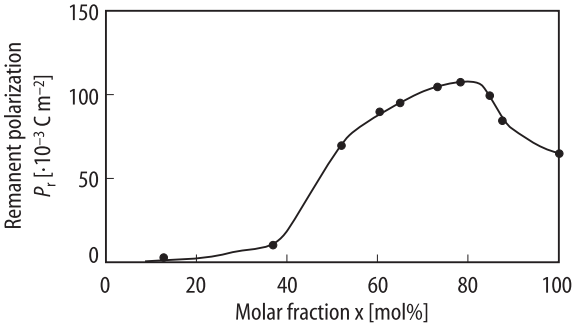

Fig. 72-2-021. VDF_x–$TrFE_{1-x}$. P_r vs. x [89Fur2]. T = RT.

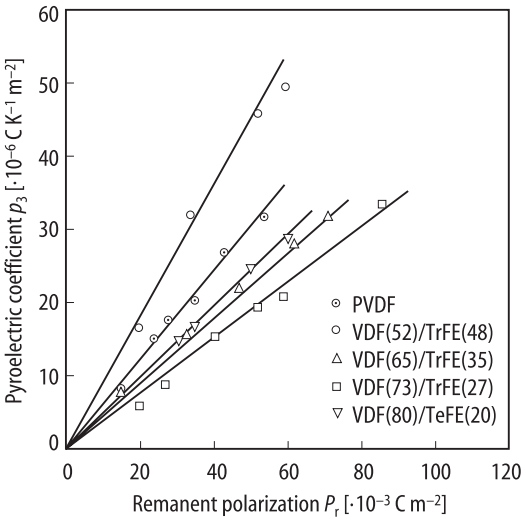

Fig. 72-2-022. VDF_x–$TrFE_{1-x}$, VDF_x–$TeFE_{1-x}$. p_3 vs. P_r [89Fur1].

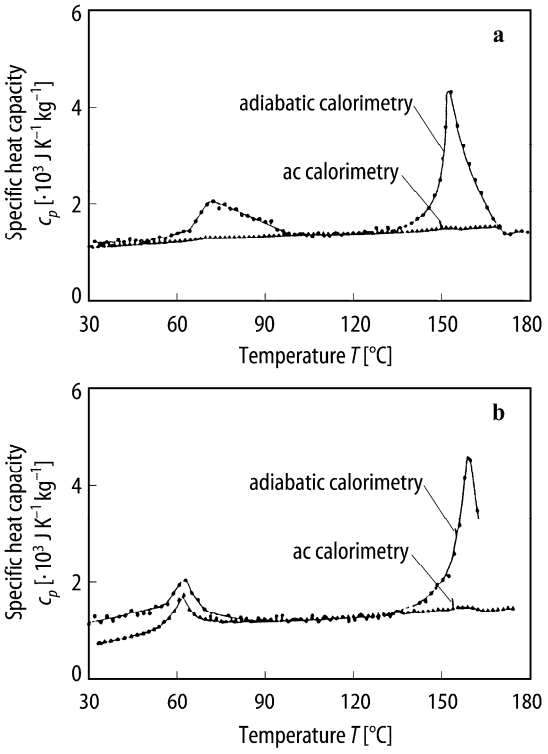

Fig. 72-2-023. VDF_x–$TrFE_{1-x}$. Adiabatic and ac specific heat vs. T [92Ogu]. (**a**) x = 0.65, (**b**) x = 0.54.

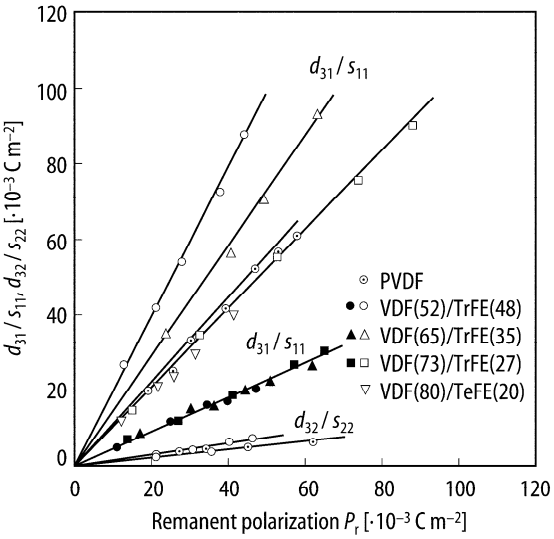

Fig. 72-2-024. VDF_x–$TrFE_{1-x}$, VDF_x–$TeFE_{1-x}$. d_{31}/s_{11} and d_{32}/s_{22} vs. P_r [89Fur1]. Parameter: x. Full symbols: undrawn samples, open symbols: drawn samples.

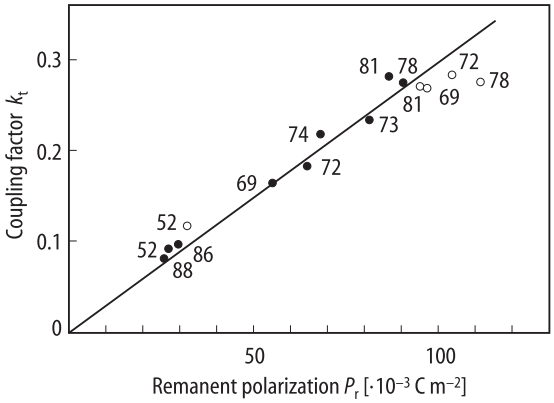

Fig. 72-2-025. VDF_x–$TrFE_{1-x}$. Coupling factor k_t vs. P_r [86Kog]. Open circle: for unstretched film, full circle: for stretched film. Numerals indicate x in VDF mol%.

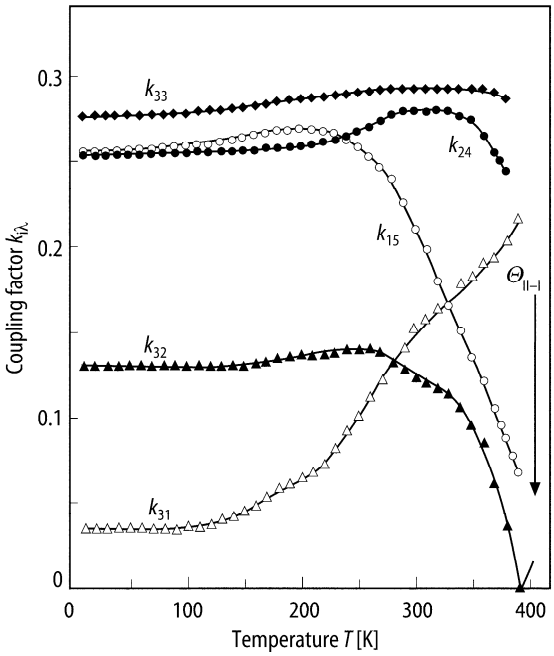

Fig. 72-2-026. VDF_x–$TrFE_{1-x}$. Coupling factors $k_{i\lambda}$ vs. T [97Omo].

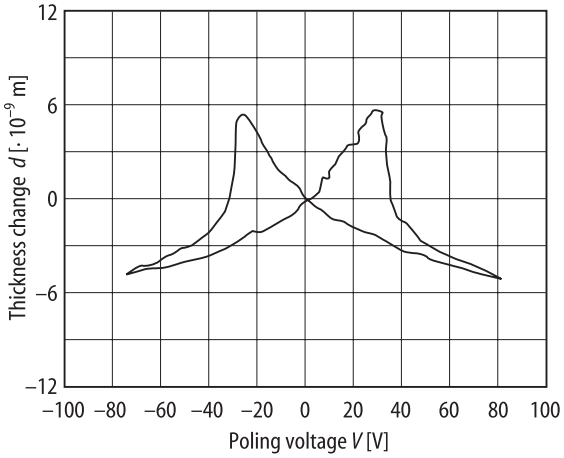

Fig. 72-2-027. VDF_x–$TrFE_{1-x}$. Thickness change d vs. poling voltage V (electrostriction) [95LiJ]. Thickness of the specimen = 0.8 µm.

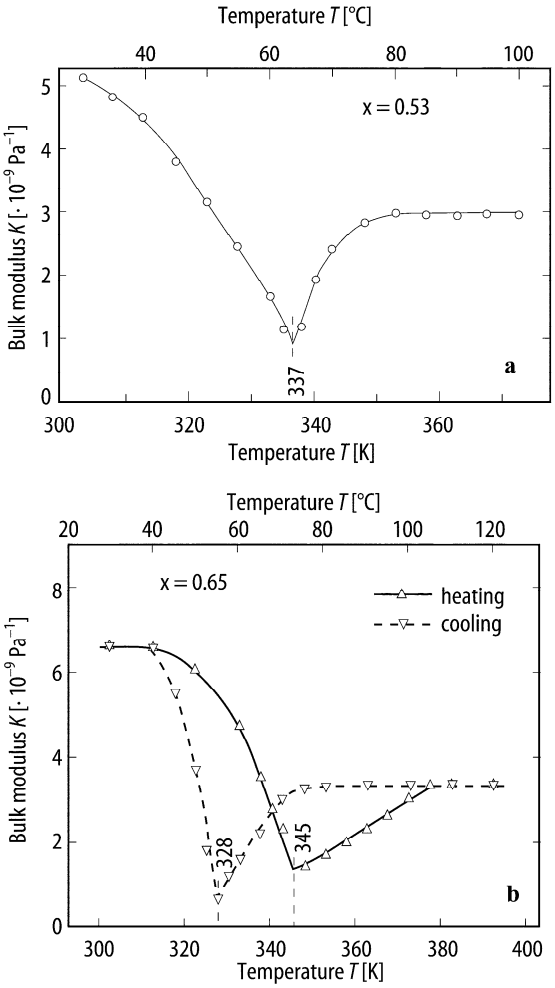

Fig. 72-2-028. VDF_x–$TrFE_{1-x}$. K vs. T [94Koi]. $K = (\Delta V/V)/p$ (bulk modulus). (**a**) x = 0.53, (**b**) x = 0.65.

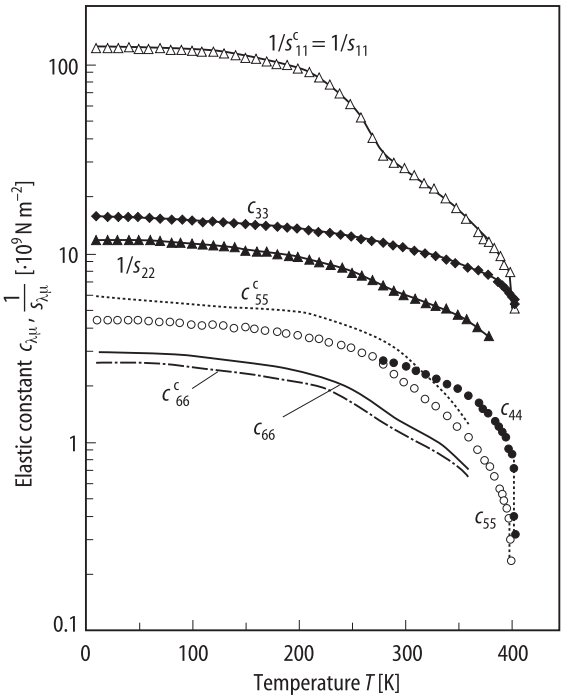

Fig. 72-2-029. $VDF_{0.75}$–$TrFE_{0.25}$. $c_{\lambda\mu}$, $1/s_{\lambda\mu}$ vs. T for a single-crystal-like film [97Omo]. $c^c_{\lambda\mu}$, $1/s^c_{\lambda\mu}$: for a single crystal.

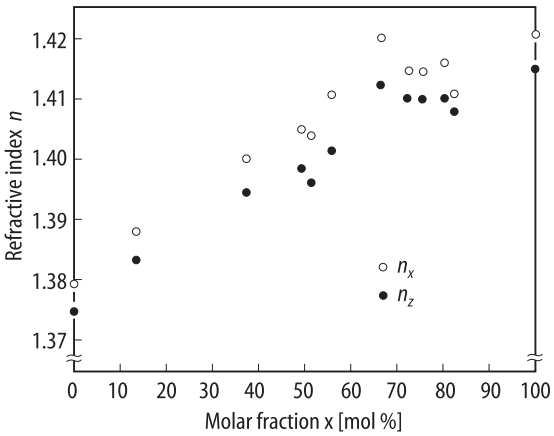

Fig. 72-2-030. VDF_x–$TrFE_{1-x}$. Refractive indices vs. x [82Yam].

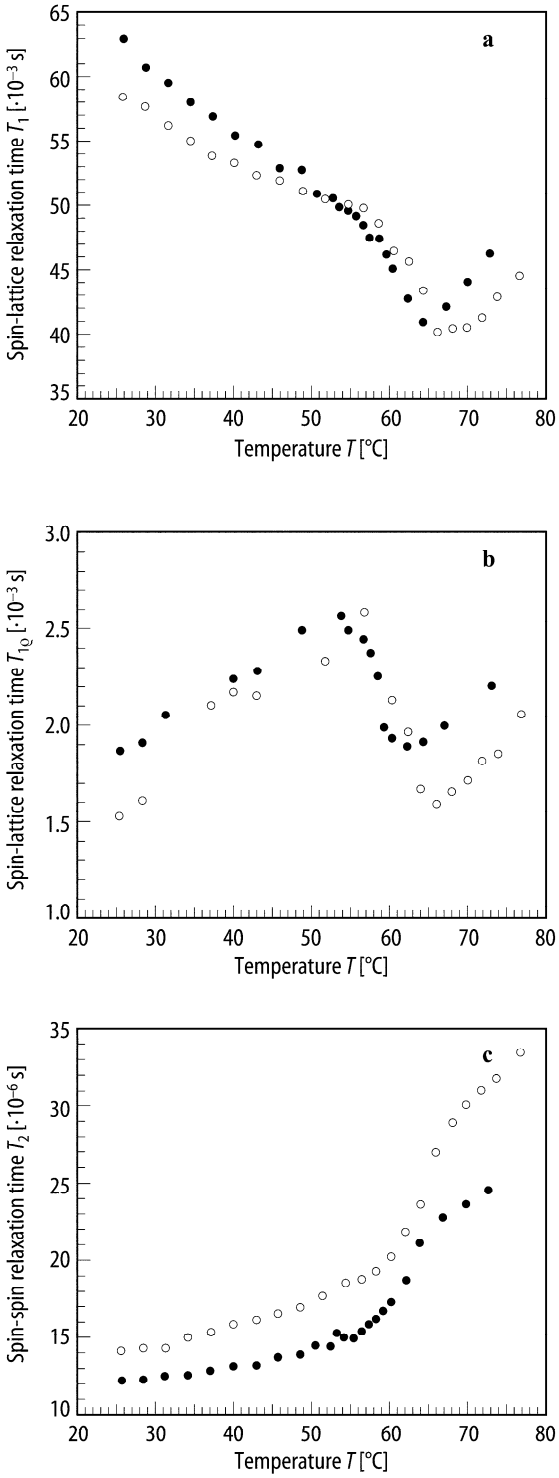

Fig. 72-2-031. $VDF_{0.55}$–$TrFE_{0.45}$. (**a**) T_1 vs. T, (**b**) $T_{1\rho}$ vs. T, (**c**) T_2 vs. T [89Tan]. Open circle: for quenched sample, full circle: for isothermally crystallized sample.

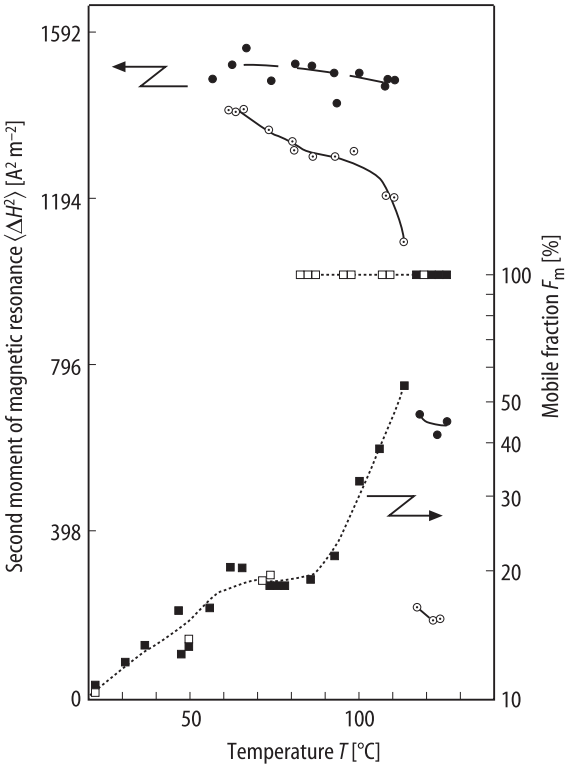

Fig. 72-2-032. $VDF_{0.73}$–$TrFE_{0.27}$. $<\Delta H^2>$ vs. T, F_m vs. T [83Ish]. F_m: mobile fraction. For $<\Delta H^2>$, full circle: $\gamma = 0°$, open circle with a dot in centre: $\gamma = 90°$. γ: angle between $\boldsymbol{H}_0$ and an axis in the film. For F_m, $\gamma = 0°$ and full square: increasing T from 23 °C to 130 °C, open square: decreasing T from 130 °C to 23 °C.

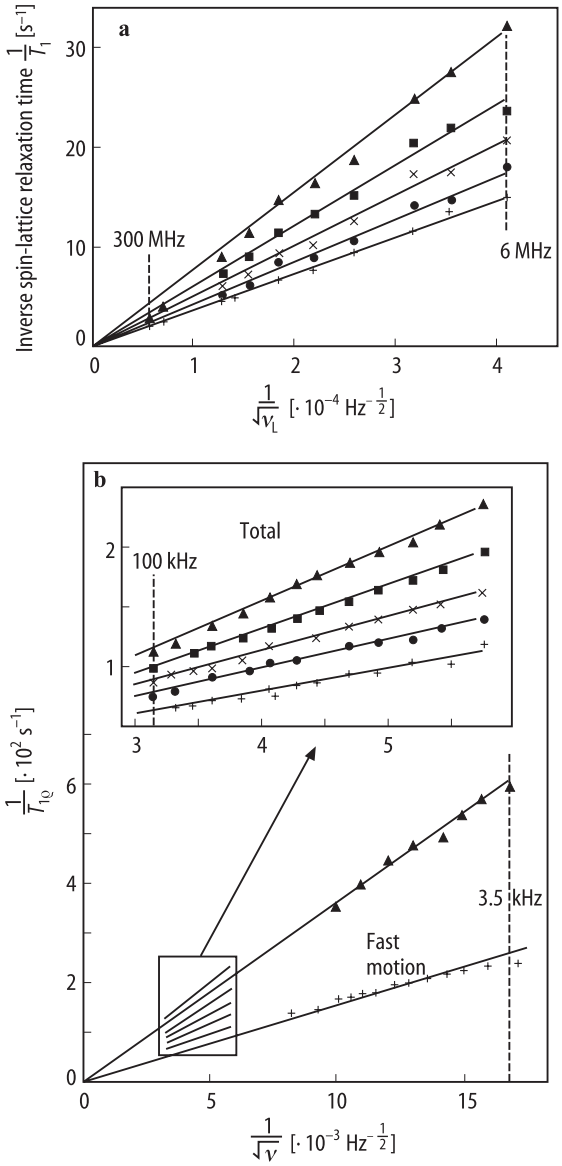

Fig. 72-2-033. $VDF_{0.7}$–$TrFE_{0.3}$. (**a**) $1/T_1$ vs. $1/\sqrt{\nu_L}$, (**b**) $1/T_{1\rho}$ vs. $1/\sqrt{\nu}$ for ^1H [83Ish]. Parameter: *T*. Full triangle: $T = 80$ °C, full square: $T = 90$ °C, cross: $T = 100$ °C, full circle: $T = 110$ °C, plus: $T = 120$ °C.

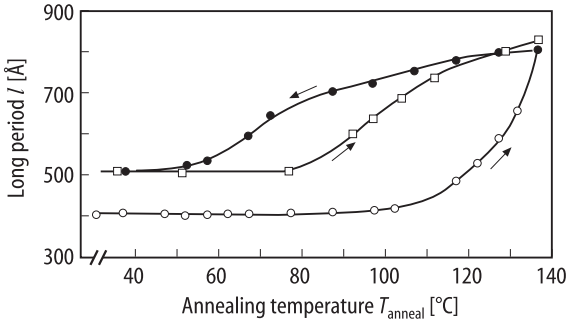

Fig. 72-2-034. $VDF_{0.7}$–$TrFE_{0.3}$. l vs. T_{anneal} [91Bou]. l: long period in lamellar stacking measured by X-ray small angle scattering. T_{anneal}: annealing temperature. Open circle: first heating run, full circle: cooling run, square: second heating run.

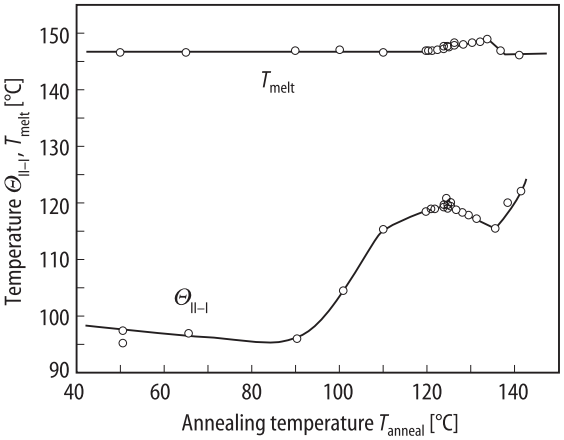

Fig. 72-2-035. $VDF_{0.73}$–$TrFE_{0.27}$. Θ_{II-I}, T_{melt} vs. T_{anneal} [95Tas]. T_{anneal}: annealing temperature.

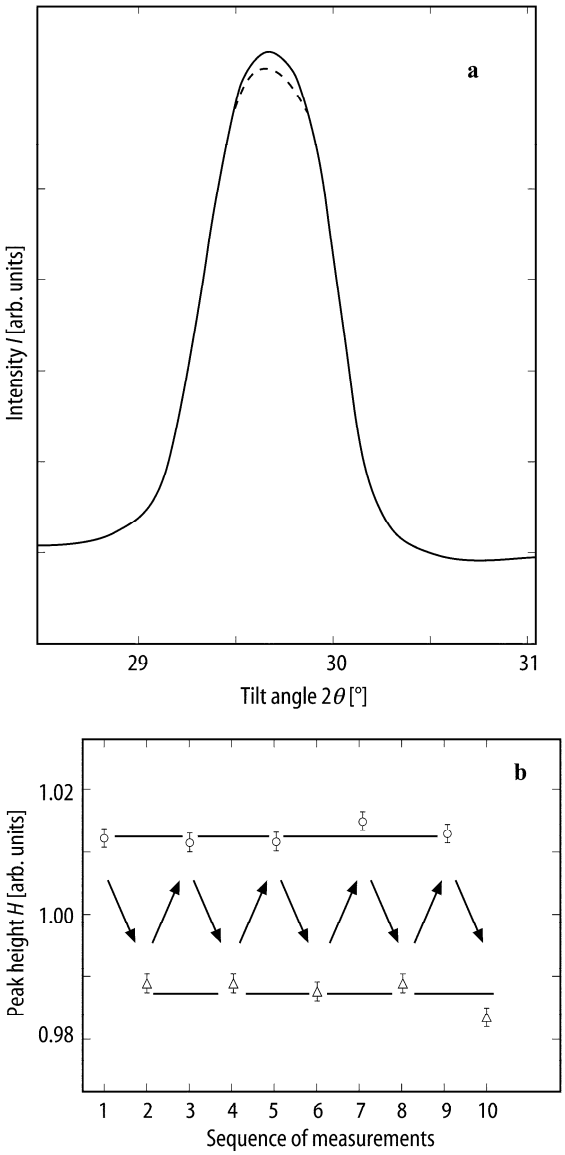

Fig. 72-2-036. $VDF_{0.65}$–$TrFE_{0.35}$. Change in X-ray diffraction intensity associated with polarization switching [87Tak]. (**a**) Difference between the solid and dashed lines indicates the change by polarization switching. (**b**) Changes of the peak height *H* following the sequence of switchings indicated by arrows.

References

80Fur Furukawa, T., Date, M., Fukada, E., Tajitsu, Y., Chiba, A.: Jpn. J. Appl. Phys. **19** (1980) L109.
80Kit Kitayama, T., Ueda, T., Yamada, T.: Ferroelectrics **28** (1980) 301.
80Yag Yagi, T., Tatemoto, M., Sako, J.: Polym. J. **12** (1980) 209.
82Lov Lovinger, A.J., Davis, G.T., Furukawa, T., Broadhurst, M.G.: Macromolecules **15** (1982) 323.
82Yam Yamada, T., Kurokawa, T.: Appl. Phys. Lett. **40** (1982) 361.
83Ish Ishii, F., Odajima, A., Ohigashi, H.: Polym. J. **15** (1983) 875.
83Kim Kimura, K., Ohigashi, H.: Appl. Phys. Lett. **43** (1983) 834.
83Lov1 Lovinger, A.J., Furukawa, T., Davis, G.T., Broadhurst, M.G.: Polymer **24** (1983) 1225.
83Lov2 Lovinger, A.J., Furukawa, T., Davis, G.T., Broadhurst, M.G.: Polymer **24** (1983) 1233.
84Fur1 Furukawa, T., Ohuchi, M., Chiba, A., Date, M.: Macromolecules **17** (1984) 1384.
84Fur2 Furukawa, T.: Ferroelectrics **57** (1984) 63.
84Koi Koizumi, N., Haikawa, N., Habuka, H.: Ferroelectrics **57** (1984) 99.
84Tas Tashiro, K., Takano, K., Kobayashi, M., Chatani, Y., Tadokoro, H.: Ferroelectrics **57** (1984) 297.
85Leg Legrand, J.F., Schuele, P.J., Schmidt, V.H., Minier, M.: Polymer **26** (1985) 1683.
86Ish1 Ishii, F., Odajima, A.: Polym. J. **18** (1986) 547.
86Ish2 Ishii, F., Odajima, A.: Polym. J. **18** (1986) 539.
86Kog Koga, K., Ohigashi, H.: J. Appl. Phys. **59** (1986) 2142.
86Koi Koizumi, N., Murata, Y., Tsunashima, H.: IEEE Trans. Electr. Insul. **21** (1986) 543.
87Fer Fernandez, M.V., Suzuki, A., Chiba, A.: Macromolecules **20** (1987) 1806.
87Hir Hirschinger, J., Meurer, B., Weill, G.: Polymer **28** (1987) 721.
87Ogu Ogura, H., Chiba, A.: Ferroelectrics **74** (1987) 347.
87Tak Takahashi, Y., Nakagawa, Y., Miyaji, H., Asai, K.: J. Polym. Sci. Part C **25** (1987) 153.
88Pet Petzelt, J., Legrand, J.F., Pacesova, S., Kamba, S.: Phase Transitions **12** (1988) 305.
88Sta Stack, G.M., Ting, R.Y.: J. Polym. Sci. Part B **26** (1988) 55.
88Tan Tanaka, H., Yukawa, H., Nishi, T.: Macromolecules **21** (1988) 2469.
88Tas Tashiro, K., Nishimura, S., Kobayashi, M.: Macromolecules **21** (1988) 2463.
89Ber Berge, B., Wicker, A., Lajzerowicz, J., Legrand, J.F.: Europhys. Lett. **9** (1989) 657.
89Fur1 Furukawa, T.: IEEE Trans. Electr. Insul. **24** (1989) 375.
89Fur2 Furukawa, T.: Phase Transitions **18** (1989) 143.
89Hir Hirschinger, J., Meurer, B., Weill, G.: J. Phys. (Paris) **50** (1989) 583.
89Mat Matsushige, K.: Phase Transitions **18** (1989) 247.
89Per Perry, C., Dratz, E.A., Ke, Y., Schmidt, V.H., Kometani, J.M.: Ferroelectrics **92** (1989) 55.
89Tan Tanaka, H., Yukawa, H., Nishi, T.: J. Chem. Phys. **90** (1989) 6740.
89Tas Tashiro, K., Kobayashi, M.: Phase Transitions **18** (1989) 213.
90Fur Furukawa, T., Seo, N.: Jpn. J. Appl. Phys. **29** (1990) 675.
90Kog Koga, K., Ohigashi, H.: J. Appl. Phys. **67** (1990) 965.
90Leg Legrand, J.F., Frick, B., Meurer, B., Schmidt, V.H., Bee, M., Lajzerowicz, J.: Ferroelectrics **109** (1990) 321.
90Ogu Ogura, H., Kase, K.: Ferroelectrics **110** (1990) 145.
91Bou Bourgaux-Leonard, C., Legrand, J.F., Renault, A., Delzenne, P.: Polymer **32** (1991) 597.
91Dau Daubin, B., Legran, J.F., Macchi, F.: J. Appl. Phys. **70** (1991) 4037.
91Ike Ikeda, S., Kutani, M., Fukaya, T., Kominami, H.: Polym. J. **23** (1991) 327.
92Day Day, J.A., Lewis, E.L., Davies, G.R.: Polymer **33** (1992) 1571.
92Fur Furukawa, T., Tajitsu, Y., Zhang, X., Johnson, G.E.: Ferroelectrics **135** (1992) 401.
92Gue Guethner, P., Ritter, T., Dransfeld, K.: Ferroelectrics **127** (1992) 7.
92Miz Mizuno, H., Nagano, Y., Tashiro, K., Kobayashi, M.: J. Chem. Phys. **96** (1992) 3234.
92Ogu Ogura, H., Shimizu, T., Motoyama, H., Ochiai, M., Chiba, A.: Jpn. J. Appl. Phys. **31** (1992) 835.
93Kru Krueger, J.K., Prechtl, M., Wittmann, J.C., Meyer, S., Legrand, J.F., D'Asseza, G.: J. Polym. Sci. Part B **31** (1993) 505.
94Bel Bellet-Amalric, E., Legrand, J.F., Stock-Schweyer, M., Meurer, B.: Polymer **35** (1994) 34.
94Kim Kim, K.J., Kim, G.B., Valencia, C.L., Rabolt, J.F.: J. Polym. Sci. Part B **32** (1994) 2435.
94Koi Koizumi, N.: Key Eng. Mater. **92-93** (1994) 161.

95Fur Furukawa, T., Kodama, H., Uchinokura, O., Takahashi, Y.: Ferroelectrics **171** (1995) 33.
95Isn Isner-Brom, P., Brissaud, M., Heintz, R., Eyraud, L., Bauer, F.: Ferroelectrics **171** (1995) 271.
95LiJ Li, J., Baur, C., Koslowski, B., Dransfeld, K.: Physica **B204** (1995) 318.
95Omo Omote, K., Ohigashi, H.: Appl. Phys. Lett. **66** (1995) 2215.
95Sas Sasaki, S., Funato, A., Kubo, K., Chiba, A.: Jpn. J. Appl. Phys. **34** (1995) 3177.
95Tas Tashiro, K., Tanaka, R., Ushitora, K., Kobayashi, M.: Ferroelectrics **171** (1995) 143.
97Omo Omote, K., Ohigashi, H., Koga, K.: J. Appl. Phys. **81** (1997) 2760.
97Taj Tajitsu, Y., Fujii, M., Suzuki, H., Aoki, M., Suzuki, K., Ohigashi, H.: Jpn. J. Appl. Phys. **36** (1997) L693.
01Fur Furukawa, T., Takahashi, Y.: Ferroelectrics **264** (2001) 1739.

No. 72-3 $((CH_2CF_2)_x(CF_2CF_2)_{1-x})_n$, Vinylidene fluoride-tetrafluoroethylene copolymer (VDF_x–$TeFE_{1-x}$, VDF–TeFE)

1a	Ferroelectric hysteresis loops were observed in films of random copolymers $((CH_2CF_2)_x(CF_2CF_2)_{1-x})_n$ for x = 0.8 by Hicks et al. in 1978.	78Hic
b	Phase diagram: Fig. 72-3-001.	
3a	d_{110} (or d_{200}) vs. x: Fig. 72-3-002.	
4	d_{110} (or d_{200}) vs. T: Fig. 72-3-003.	
5a	Dielectric properties: see	78Hic, 84Lov
	$\kappa_0 - \kappa_\infty$ and τ vs. T: Fig. 72-3-004.	
b	D–E hysteresis loop, see	78Hic, 85Wen, 94Koi
d	p_3 vs. poling field: Fig. 72-3-005.	
	p_3 vs. P_r: see Fig. 72-2-022 and see also	89Fur
6a	DSC thermogram: Fig. 72-3-006.	
7a	d_{31} and d_{32} vs. T: Fig. 72-3-007.	
	d_{31} vs. P_r, see Fig. 72-2-024.	
8a	Sound velocity vs. T: Fig. 72-3-008.	
	Elastic dispersion: see	85Mur

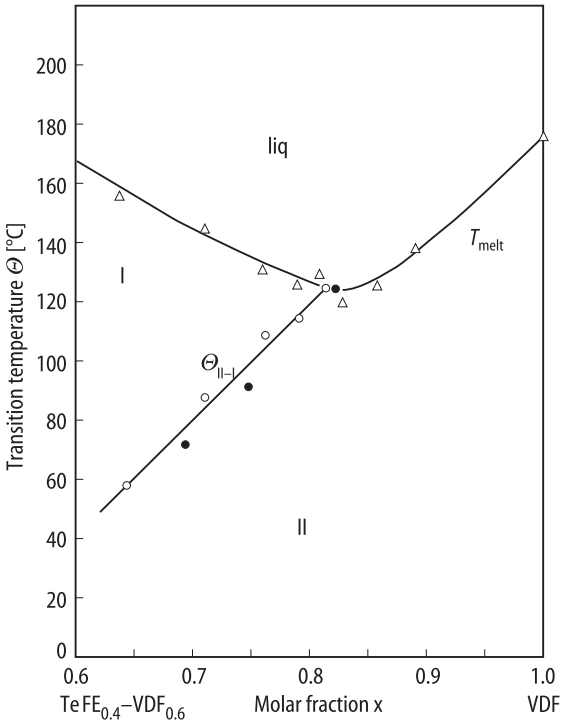

Fig. 72-3-001. VDF$_x$–TeFE$_{1-x}$. Phase diagram, Θ vs. x [86Lov]. Open triangle, open circle: by [86Lov], full circle: by [85Mur]. Θ_{II-I} was determined by X-ray diffraction.

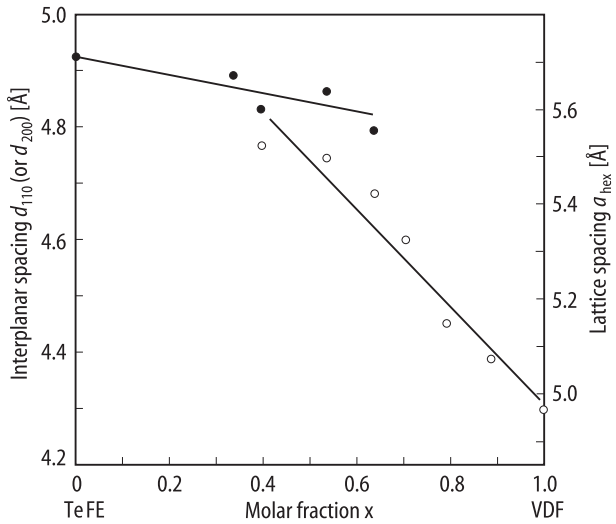

Fig. 72-3-002. VDF$_x$–TeFE$_{1-x}$. d_{110} (or d_{200}), a_{hex} vs. x [88Lov]. Full circle: d_{110} (or d_{200}), open circle: a_{hex}, reduced lattice spacing. At intermediate compositions, two hexagonal phases coexist.

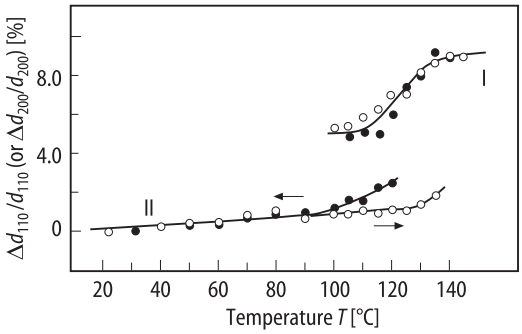

Fig. 72-3-003. VDF_x–$TeFE_{1-x}$. $\Delta d_{110}/d_{110}$ (or $\Delta d_{200}/d_{200}$) vs. T associated with ferroelectric transition [92Tas]. Open circle: heating, full circle: cooling. I: paraelectric, II: ferroelectric.

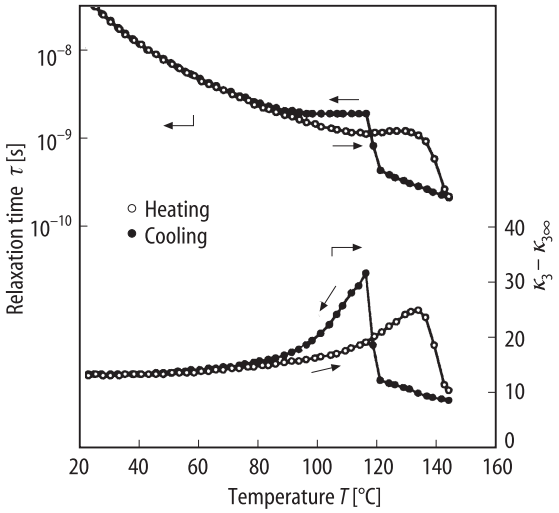

Fig. 72-3-004. $VDF_{0.81}$–$TeFE_{0.19}$. $\kappa_3 - \kappa_{3\infty}$ and τ vs. T [92Fur]. $\kappa_{3\infty}$: κ_3 at high frequency. τ: relaxation time. Ferroelectric transition is overtaken by melting at 135 °C.

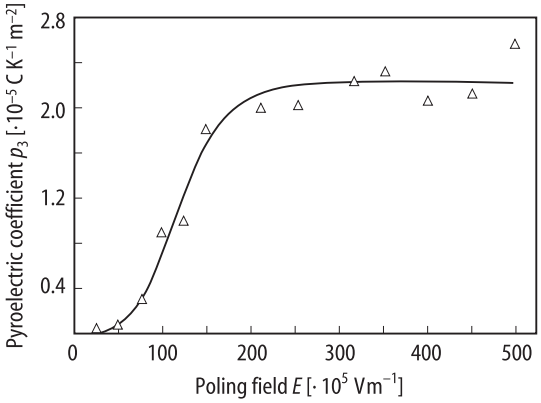

Fig. 72-3-005. $VDF_{0.73}$–$TeFE_{0.27}$. p_3 vs. poling field E [82Bro].

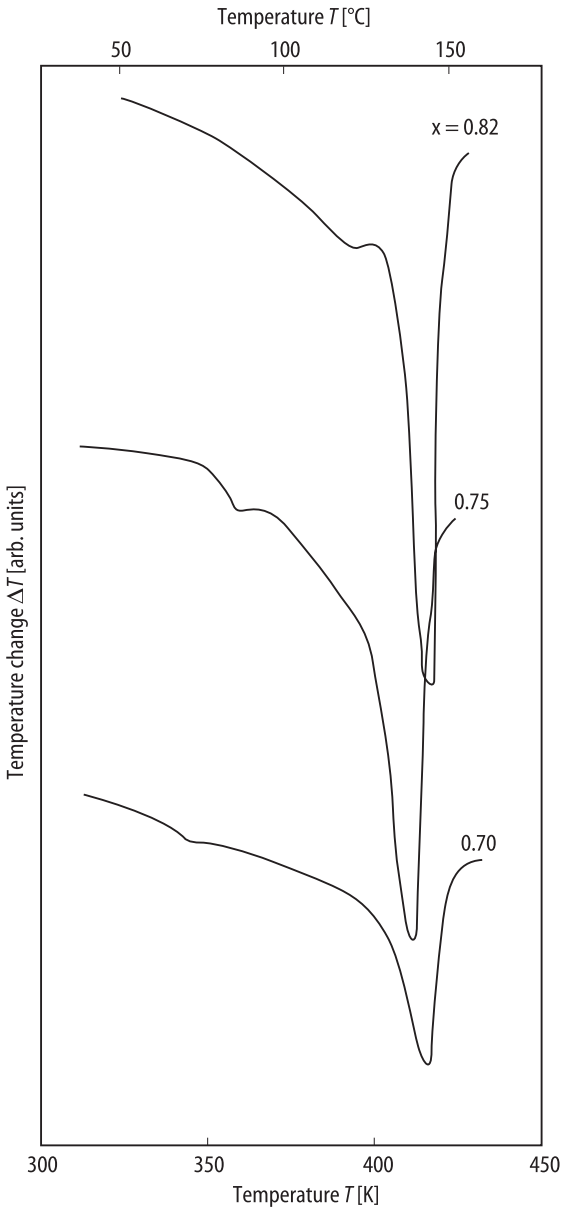

Fig. 72-3-006. VDF_x–$TeFE_{1-x}$. DSC thermogram [85Mur]. Parameter: x.

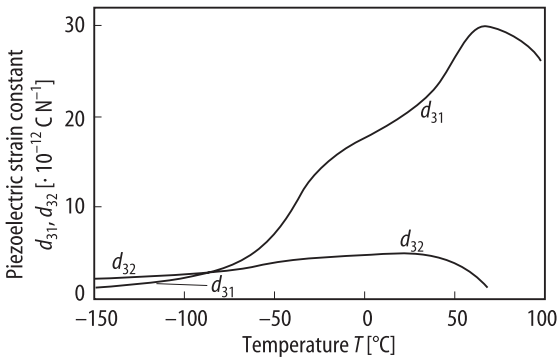

Fig. 72-3-007. $VDF_{0.8}$–$TeFE_{0.2}$. d_{31} and d_{32} vs. T [85Wen].

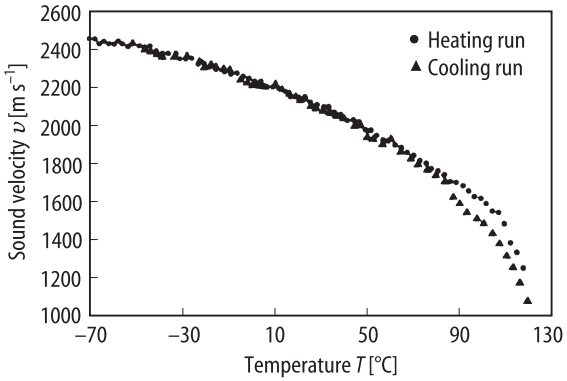

Fig. 72-3-008. $VDF_{0.81}$–$TeFE_{0.19}$. v vs. T. v: sound velocity measured by Brillouin spectroscopy [90Liu].

References

78Hic Hicks, J.C., Jones, T.E., Logan, J.C.: J. Appl. Phys. **49** (1978) 6092.
82Bro Broadhurst, M., Davis, G.T., DeReggi, A.S., Roth, S.C., Colloins, R.E.: Polymer **23** (1982) 22.
84Lov Lovinger, A.J., Johnson, G.E., Bair, H.E., Anderson, E.W.: J. Appl. Phys. **56** (1984) 2412.
85Mur Murata, Y., Koizumi, N.: Polym. J. **17** (1985) 1071.
85Wen Wen, J.X.: Polym. J. **17** (1985) 399.
86Lov Lovinger, A.J., Davis, D.D., Cais, R.E., Kometani, J.M.: Macromolecules **19** (1986) 1491.
88Lov Lovinger, A.J., Davis, D.D., Cais, R.E., Kometani, J.M.: Macromolecules **21** (1988) 78.
89Fur Furukawa, T.: IEEE Trans. Electr. Insul. **24** (1989) 375.
90Liu Liu, Z., Schmidt, H.: Ferroelectrics **112** (1990) 237.
92Fur Furukawa, T., Tajitsu, Y., Zhang, X., Johnson, G.E.: Ferroelectrics **135** (1992) 401.
92Tas Tashiro, K., Kato, H., Kobayashi, M.: Polymer **33** (1992) 2915.
94Koi Koizumi, N.: Key Eng. Mater. **92-93** (1994) 161.

No. 72-4 Odd Nylons $(NH(CH_2)_{x-1}CO)_n$ (nylon x) with x = 5, 7, 9, 11

1a	Ferroelectric hysteresis loop was found in melt-quenched and uniaxially-drawn odd nylons by Lee et al. in 1991.	91Lee
2a	Rapid cooling odd numbered nylons from the melt (200 °C) followed by uniaxial-drawing four times the original length at room temperature produces ferroelectric film. Annealing at elevated temperatures causes loss of ferroelectricity.	91Lee
3a	Melt-quenched and uniaxially-drawn ferroelectric nylon films exhibit diffuse X-ray diffraction, which indicates that molecules with skew or gauche conformation are packed in a pseudohexagonal lattice.	94Bal, 97Tak
b	Lattice spacing vs. annealing temperature: see	97Tak
5a	Dielectric constant vs. temperature: Fig. 72-4-001.	
c	*D–E* hysteresis loops of nylon 11: Fig. 72-4-002. P_r vs. annealing temperature: Fig. 72-4-003. P_r vs. dipole density: Fig. 72-4-004. Switching characteristics of nylon 11: Fig. 72-4-005.	
7a	d_{31} and d_{32} vs. T: Fig. 72-4-006. k_{33} vs. P_r: Fig. 72-4-007.	
8a	Temperature variation of Young's modulus: see	91Tak
15	Electric-field induced structural changes: see	84Jac, 95Mei, 97Tsu

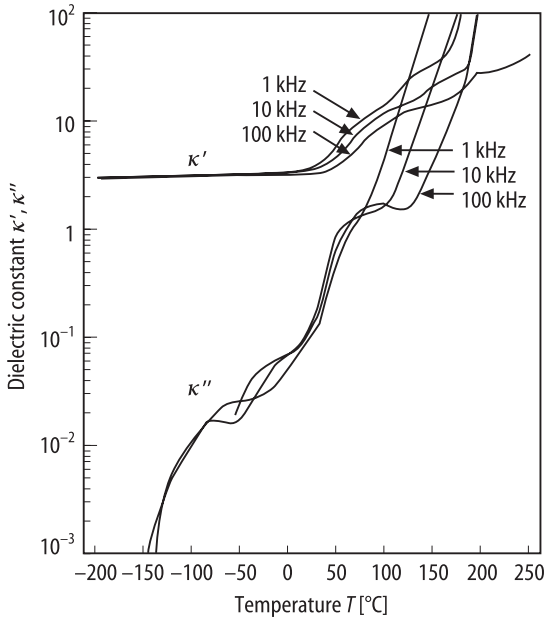

Fig. 72-4-001. Odd Nylon. κ', κ'' vs. T in nylon 11 [91Tak]. Parameter: frequency f.

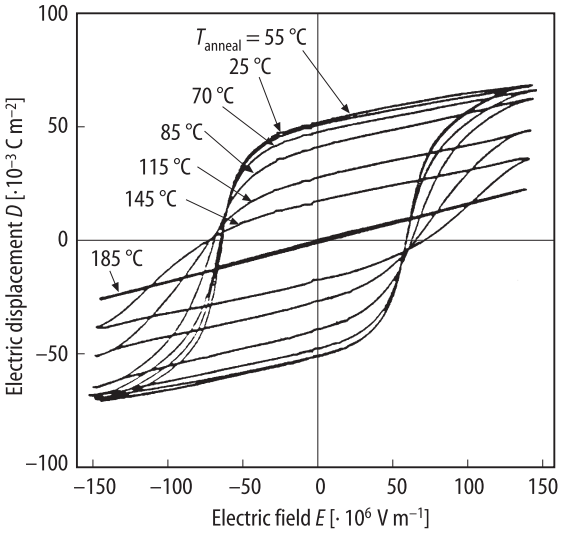

Fig. 72-4-002. Odd Nylon. D–E hysteresis loops of nylon 11 films as-drawn and annealed [91Lee]. Parameter: T_{anneal}.

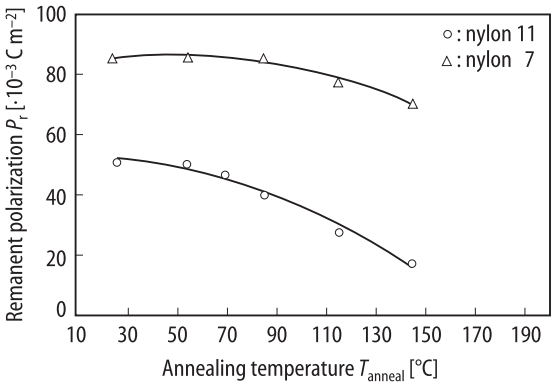

Fig. 72-4-003. Odd Nylon. P_r vs. T_{anneal} in nylon 7 and 11 [91Lee].

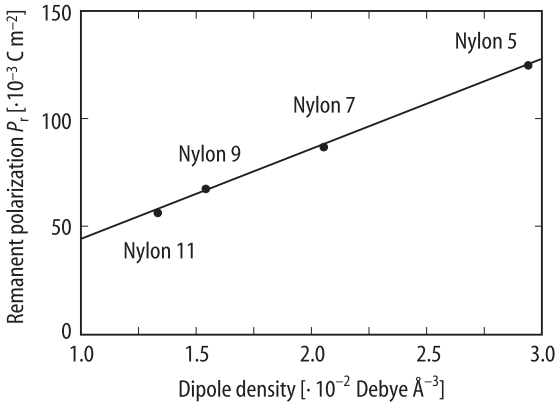

Fig. 72-4-004. Odd Nylon. P_r vs. dipole density for x = 5, 7, 9 and 11 [93Mei].

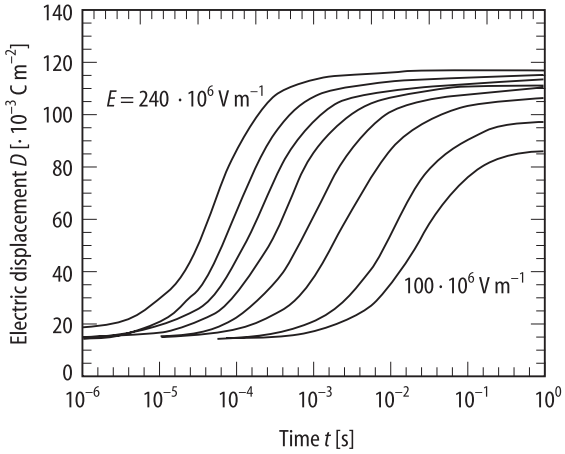

Fig. 72-4-005. Odd Nylon. Switching characteristics of nylon 11 [95Ike]. Parameter: applied electric field at step of 20 MV/m.

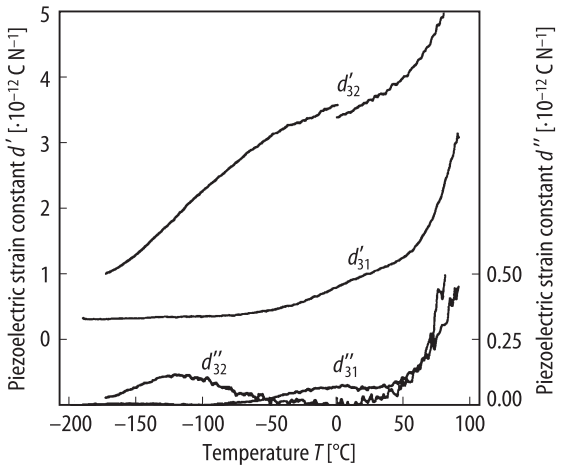

Fig. 72-4-006. Odd Nylon. $d'_{i\lambda}$, $d''_{i\lambda}$ vs. T [91Tak]. $d'_{i\lambda}$, $d''_{i\lambda}$: real and imaginary parts of complex piezoelectric strain constant, $d^*_{i\lambda} = d'_{i\lambda} - \mathrm{i}d''_{i\lambda}$.

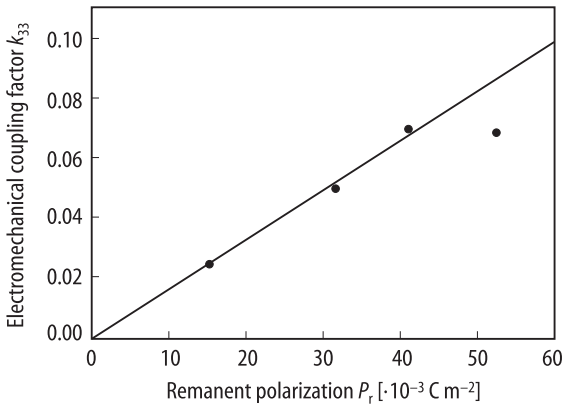

Fig. 72-4-007. Odd Nylon. k_{33} vs. P_r of nylon 11 [95Shi]. k_{33}: electromechanical coupling factor.

References

84Jac Jacobs, E.W., Hicks, J.C.: Appl. Phys. Lett. **44** (1984) 402.

91Lee Lee, J.W., Takase, Y., Newman, B.A., Scheinbeim, J.I.: J. Polym. Sci. Part B **29** (1991) 279.

91Tak Takase, Y., Lee, J.W.: Macromolecules **24** (1991) 6644.

93Mei Mei, B.Z., Scheinbeim, J.I., Newman, B.A.: Ferroelectrics **144** (1993) 51.

94Bal Balizer, E., Fedderly, J., Haught, D., Dickens, B., DeReggi, A.S.: J. Polym. Sci. Part B **32** (1994) 365.

95Ike Ikeda, S., Saito, T., Nonomura, M., Koda, T.: Ferroelectrics **171** (1995) 329.

95Mei Mei, B.Z., Scheinbeim, J.I., Newman, B.A.: Ferroelectrics **171** (1995) 177.

95Shi Shimomura, M., Takahashi, Y., Furukawa, T.: Polym. Prep. Jpn. **44** (1995) 3411.

97Tak Takahashi, Y., Shimomura, M., Kutani, M., Furukawa, T.: Polym. J. **29** (1997) 234.

97Tsu Tsurutani, N., Miyaji, H., Izumi, K., Tasaka, S.: Polymer **38** (1997) 2881.

No. 72-5 poly-m-Xylylene adipamide

1a	Ferroelectric hysteresis loops were observed in thin films of poly-m-xylylene adipamide by Murata et al. in 1993.	93Mur
5c	*D–E* hysteresis loop: Fig. 72-5-001.	

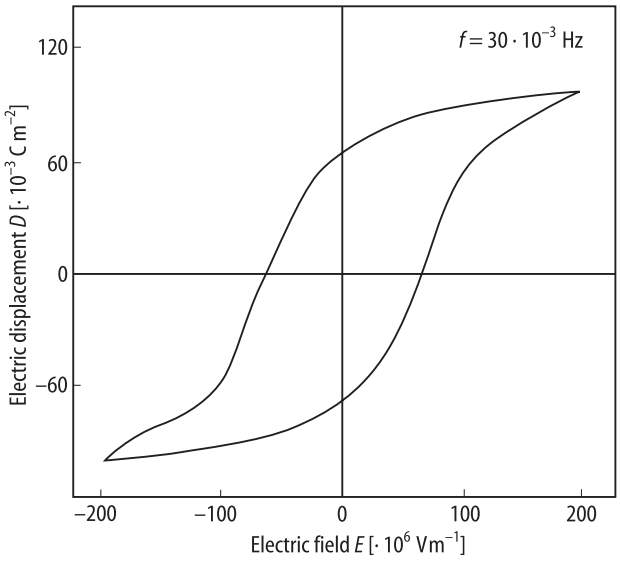

Fig. 72-5-001. poly-m-Xylylene adipamide. *D*–*E* hysteresis loop [93Mur].

Reference

93Mur Murata, Y., Tsunashima, K., Koizumi, N., Ogami, K., Hosokawa, F., Yokoyama, K.: Jpn. J. Appl. Phys. **32** (1993) L849.